NEOPLASIA
www.neoplasia.com

Volume 18 Number 8 August 2016 pp. 512–523 512

NHERF1/EBP50 Suppresses Wnt-β-Catenin Pathway–Driven Intestinal Neoplasia[1]

Maria-Magdalena Georgescu*, Mihai Gagea† and Gilbert Cote‡

*Department of Pathology and Translational Pathobiology, Louisiana State University, Shreveport, LA, 71103, USA; †Department of Veterinary Medicine, The University of Texas MD Anderson Cancer Center, Houston, TX, 77030, USA; ‡Department of Endocrine Neoplasia and Hormonal Disorders, The University of Texas MD Anderson Cancer Center, Houston, TX, 77030, USA

Abstract

NHERF1/EBP50, an adaptor molecule that interacts with β-catenin, YAP, and PTEN, has been recently implicated in the progression of various human malignancies, including colorectal cancer. We report here that NHERF1 acts as a tumor suppressor *in vivo* for intestinal adenoma development. NHERF1 is highly expressed at the apical membrane of mucosa intestinal epithelial cells (IECs) and serosa mesothelial cells. *NHERF1*-deficient mice show overall longer small intestine and colon that most likely could be attributed to a combination of defects, including altered apical brush border of absorbtive IECs and increased number of secretory IECs. *NHERF1* deficiency in *Apc*$^{Min/+}$ mice resulted in significantly shorter animal survival due to markedly increased tumor burden. This resulted from a moderate increase of the overall tumor density, more pronounced in females than males, and a massive increase in the number of large adenomas in both genders. The analysis of possible pathways controlling tumor size showed upregulation of Wnt-β-catenin pathway, higher expression of unphosphorylated YAP, and prominent nuclear expression of cyclin D1 in NHERF1-deficient tumors. Similar YAP changes, with relative decrease of phosphorylated YAP and increase of nuclear YAP expression, were observed as early as the adenoma stages in the progression of human colorectal cancer. This study discusses a complex role of NHERF1 for intestinal morphology and presents indisputable evidence for its *in vivo* tumor suppressor function upstream of Wnt-β-catenin and Hippo-YAP pathways.

Neoplasia (2016) 18, 512–523

Introduction

Human colorectal cancer (CRC) is the third most common type of cancer and the third cause of mortality due to cancer in the United States [1]. It typically evolves from a benign polyp, or adenoma, to malignant carcinoma that starts in the mucosa [carcinoma in situ; American Joint Committee on Cancer (AJCC) stage 0] and spreads through the other layers of the colon or rectum. In advanced stages, malignant cells metastasize to the lymph nodes (AJCC stage III) or to distant organs (AJCC stage IV). The ability of CRC cells to invade and metastasize renders the tumors unresectable and resistant to chemotherapy and diminishes abruptly the overall survival rate to approximately 10% at 5 years for AJCC stage IV patients [2].

The understanding of the progression of CRC sets the foundation for the development of therapeutic approaches. Approximately 85% of sporadic CRCs have deregulation of the canonical Wnt-β-catenin pathway, the same central pathway that is involved in intestinal epithelial cell (IEC) renewal [3]. Wnt3, 6, and 9B expressed only in the crypt epithelium bind to Frizzled transmembrane receptors and to low-density lipoprotein receptor–related proteins-5/6 [4]. They activate the pathway by disassembling the cytoplasmic destruction complex formed by axin, Apc, GSK-3β, CK1α/ε, and β-catenin [5,6]. In this complex, CK1 and GSK-3β phosphorylate β-catenin on N-terminal residues and target it for proteasome degradation.

Abbreviations: H&E, hematoxylin and eosin; IEC, intestinal epithelial cell; IF, immunofluorescence; IHC, immunohistochemistry; CRC, colorectal cancer; ERM, ezrin-radixin-moesin; NHERF1/EBP50, Na^+/H^+, exchanger 3 regulating factor 1; ERM, binding phosphoprotein 50; PI3K, phosphoinositol 3-OH kinase; PM, plasma membrane; SI, small intestine; YAP, Yes-associated protein (also known as YAP65)

Address all correspondence to: Maria-Magdalena Georgescu, Louisiana State University, 1501 Kings Highway, Shreveport, LA, 71103.
E-mail: mmgeorgescu@yahoo.com

[1] Conflict of Interest: The authors declare no conflict of interest.

Received 2 April 2016; Revised 1 July 2016; Accepted 11 July 2016

1476-5586
http://dx.doi.org/10.1016/j.neo.2016.07.003

Wnt signaling disrupts the destruction complex by removing axin and thus stabilizes β-catenin. Subsequent translocation of β-catenin to the nucleus and interaction with lymphoid enhancer factor/T-cell factor DNA-binding proteins activate the transcription of Wnt target genes [7], including cyclin D1 [8]. The almost always-present hit at the level of the β-catenin destruction complex in CRC can explain the growth of the tumors but cannot explain the phenotypic heterogeneity of CRC. Other contributions to enhance the activation of the Wnt/β-catenin pathway have been documented, either from components of the Wnt pathway itself or from parallel pathways that connect to the Wnt pathway, such as the PI3-kinase-PTEN-Akt pathway [9] or the Hippo-YAP/TAZ pathway [10,11].

We have shown that Na/H exchanger 3 (NHE3) regulatory factor 1 (NHERF1)/ ezrin-radixin-moesin (ERM) phosphoprotein 50 (EBP50), an adaptor protein that interacts with β-catenin and PTEN [12,13], is lost from the apical plasma membrane (PM) of IECs in tubular adenoma and CRC [14]. Interestingly, NHERF1 can be highly expressed in the cytoplasm in a subset of CRCs [14] and in the nucleus in invasive CRC fronts [15]. Cytoplasmic expression of NHERF1 increases cell proliferation [14]. NHERF1 suppresses the Wnt-β-catenin pathway in mouse embryonic fibroblasts [16], and its depletion from the apical PM in polarized colonic two-dimensional (2D) and 3D cell models leads to loss of cell polarity and gland morphology, disorganized solid growth, epithelial to mesenchymal transition, and increased migration [14,17]. To establish whether NHERF1 also has a role *in vivo* as modulator of CRC progression, we used the $Apc^{Min/+}$ mice that constitute the most used model for CRC development [18]. $Apc^{Min/+}$ mice have a point mutation in one *APC* allele and develop multiple intestinal neoplasia (Min) by activation of the Wnt-β-catenin pathway. Although NHERF1 deficiency by itself led only to morphological defects, such as increased intestinal length, NHERF1 deficiency in $Apc^{Min/+}$ mice led to significantly shorter animal survival due to increased tumor load. The most striking difference was a marked increase in the numbers of large adenomas. The tumors from $Apc^{Min/+}$ mice had reduced NHERF1 expression and activation of Wnt-β-catenin pathway. The complete lack of NHERF1 from $Apc^{Min/+}NHERF1^{-/-}$ tumors induced even higher Wnt-β-catenin pathway activation, higher expression of unphosphorylated YAP, and prominent nuclear cyclin D1 expression, attesting to the important suppressor contribution of NHERF1 to Wnt-β-catenin– and YAP-driven tumorigenesis.

Materials and Methods

Mice and Intestine Analysis

The *NHERF1*-deficient mice [19] were inbred in C57BL/6J background [20] and crossed to C57BL/6J $Apc^{Min/+}$ mice (The Jackson Laboratory, Bar Harbor, ME), inbred in the same C57BL/6J background. The offspring were genotyped for the *NHERF1* alleles as described [19] and for the *Apc* alleles as indicated by the vendor. Mice at various ages were euthanized by CO_2 inhalation. The entire intestinal tract was carefully dissected and measured. For tumor analysis, consensus recommendations were followed [21]. Briefly, the digestive tract was inflated and flushed with cold PBS; infused and incubated in 10% formalin for 3 hours; separated in proximal one third (duodenum and proximal jejunum), middle one third, distal one third (distal ileum), and colon; cut open longitudinally; and Swiss rolled on a paper tape with the serosa facing the tape and the proximal end in the center of the Swiss roll. Following overnight fixation in formalin and embedding, 5 levels (step sections) 0.5 mm apart were examined for each block. The numbers of neoplastic lesions, microadenomas (diameter < 1 mm), and adenomas were counted for each level, and the highest number per level was selected and scored as tumor density for each intestinal segment. The size of the tumors was measured with Leica Application Suite Version 4.3.0 software (Leica Microsystem, Switzerland) on images acquired with 2×/0.06 or 4×/0.13 objective from an Olympus BX41 microscope (Olympus America Inc., Center Valley, PA) equipped with a Leica DFC450 camera. When the adenoma was present on serial levels, the highest measurement was scored. The analysis of the intestinal lesions was performed by a certified anatomic pathologist, and the comprehensive analysis of the aged mice was performed by an experienced veterinary pathologist. The latter comprised soft tissues, such as lung, liver, kidney, spleen, stomach, and Swiss-rolled intestines, along with the decalcified osseous tissues skull, femur, and sternum.

Human Specimens

The frozen and formalin-fixed paraffin-embedded tissue resection specimens from patients with CRC were obtained from the Gastrointestinal Tumor Bank at MD Anderson Cancer Center (Houston, TX) and were previously described [14]. Matched sets of frozen specimens had the pathologist's annotations as normal, deep tumor (carcinoma), and tumor edge (adenoma). Paraffin-embedded resection specimens contain areas of adenoma, carcinoma, and adjacent normal mucosa on the same slide.

Histology, Immunohistochemistry (IHC), and Immunofluorescence (IF)

Formalin-fixed, paraffin-embedded sections were stained with hematoxylin and eosin (H&E) and Alcian blue by using standard protocols. Mouse tissue sections were processed for IHC as described [22] by using the Histomouse-Max kit (Zymed/Invitrogen, Carlsbad, CA). Primary antibodies were applied overnight in a humidified chamber at 4°C, with washing of unbound antibodies next day in PBS for 5 minutes three times. The following primary antibodies and corresponding dilutions were used: EBP50/NHERF1 1:3200 (PA1-090, ThermoFisher Scientific, Rockford, IL), β-catenin 1:300 (BD Biosciences, San Jose, CA), YAP 1:100 (4912) and P-YAP 1:2000 (13008) (Cell Signaling Technology, Danvers, MA), and cyclin D1 1:1000 (Santa Cruz Biotechnology, Santa Cruz, CA). Human tissue sections were processes for IHC as described [16]. For IF, mouse tissues were processed as for IHC, except for blockage from nonspecific binding for 30 minutes with 20% to 50% donkey serum in PBS. The NHERF1 and E-cadherin (BD Biosciences) antibodies were applied at 1:200. The secondary antibodies Alexa Fluor 488 donkey anti-rabbit IgG and Alexa Fluor 555 donkey anti-mouse IgG (Molecular Probes/Invitrogen) were then applied at 1:500 each in PBS for 45 minutes, followed by three PBS washes for 5 minutes. Finally, the slides were incubated in ToPro-3 iodide (Molecular Probes/Invitrogen) at 1:2000 in PBS for 20 minutes for nuclear staining and then washed with PBS for 5 minutes twice. The Slowfade Gold antifade reagent (Invitrogen) was used for the mounting of the slides. Images were acquired with a Zeiss 510 confocal microscope (Carl Zeiss MicroImaging, Thronwood, NY) using 40×/1.30 objective with oil immersion.

Transmission Electron Microscopy

Approximately 1-mm^3 colon mucosa samples were fixed with 3% glutaraldehyde and 2% paraformaldehyde in 0.1 M sodium cacodylate buffer (pH 7.3), postfixed with 1% osmium tetroxide,

and stained *en bloc* with 1% uranyl acetate. Samples were dehydrated in increasing concentrations of ethanol, infiltrated, embedded in Epon medium, and polymerized at 70°C for 2 days. Ultrathin sections were stained with uranyl acetate and lead citrate and examined in a JEM 1010 transmission electron microscope (JEOL USA Inc., Peabody, MA). Digital images were obtained by using AMT Image System (Advanced Microscopy Techniques, Danvers, MA).

BrdU Labeling

NHERF1 wild-type and mutant mice were injected intraperitoneally with 0.1 ml/10 g body weight of BrdU (Invitrogen), and sacrificed 2 hours later. Organs were harvested, fixed in 10% formalin overnight, and processed for IHC with the Animal Research Kit (Dako, Carpinteria, CA).

Plasmids, Transfections, and Protein Analysis

Human cDNAs for full-length NHERF1 and for the PDZ1 and PDZ2 domains were previously described [13]. They were inserted in frame with an Myc tag in the pcDNA3 vector. FLAG-tagged YAP wild type and YAP-S127A mutant in pCMV vector were kind gifts of Dr. K. Bhat, MD Anderson Cancer Center. The control short hairpin RNA (shRNA) and NHERF1 shRNA-1 and 4 in pSIREN-RetroQ vector and the protocol for retroviral infection of human Caco-2 CRC cells were previously described [14]. The protocols for 293T human embryonic kidney cells transfection, cell lysis, immunoprecipitation, and Western blot were previously described [23]. The cell lysis and Western blot analysis of human frozen samples were performed as described [14]. Subcellular fractionation in nuclear, cytoplasmic, and membrane compartments was described [16]. Antibodies for Western blot were obtained from the following: Myc: Invitrogen; FLAG (M2): Sigma-Aldrich, St. Louis, MO; YAP (4912) and P-YAP (4911): Cell Signaling Technology; PTEN (A2B1), PARP (H-250), and GAPDH (0411): Santa Cruz Biotechnology; E-cadherin: BD Biosciences; and villin: Chemicon/Millipore, Temecula, CA.

Statistics

All numerical data were examined for normality of distribution and expressed as means ± standard error of the mean (SEM) unless mentioned otherwise. Unpaired two-tailed *t* test with or without Welch correction for variances significantly different was used to analyze the differences between groups. Kaplan-Meier survival analysis using Gehan-Breslow-Wilcoxon test was plotted with the GraphPad Prism program (GraphPad Software, La Jolla, CA). The densitometric analysis was performed with ImageJ program (National Institutes of Health, Bethesda, MD). Data are representative of at least two or three independent experiments with similar results. Statistical significance was considered for $P < .05$.

Results

Altered Intestinal Length and Cell Composition in NHERF1 Deficient Mice

NHERF1 deficiency leads to morphological alterations of some specialized epithelia or epithelial-like linings in the body, including mammary gland, cohlea, and ependyma, resulting in dysfunction [20,24,25]. We have previously shown disruption of the brush border membrane and increase of goblet cells in the small intestine of *NHERF1*-deficient mice [19]. To better assess the intestinal defects, we analyzed the intestine in cohorts of approximately 19.5-month-old *NHERF1*$^{+/+}$ and *NHERF1*$^{-/-}$ littermates. Inspection showed significantly longer small intestine and colon in both male and female *NHERF1*$^{-/-}$ mice (Figure 1*A*). Complete histopathologic assessment of these mice showed a series of lesions associated with age (Supplementary Table 1). Of these, malignancies such as lymphoma and histiocytic sarcoma appeared equally distributed in *NHERF1*$^{+/+}$ and *NHERF1*$^{-/-}$ mice. Lymphoid hyperplasia was present in various locations in the majority of mice but appeared more extensive in *NHERF1*$^{-/-}$ mice. Nephropathies, such as glomerulonephritis and lymphocytic tubulointerstitial nephritis, and lymphocytic sialo- and dacryoadenitis were lesions much more commonly found in *NHERF1*$^{-/-}$ mice (Supplementary Table 1).

To examine whether the intestinal defects are developmental or adaptative, we performed a prospective analysis in cohorts of *NHERF1*$^{+/+}$ and *NHERF1*$^{-/-}$ inbred mice sacrificed at 6, 12 and 24 weeks. Of note is that a large proportion of *NHERF1*$^{-/-}$ mice have small weight at 3 weeks of age because of maternal lactation deficit [20]; therefore, the analysis of the intestine started at 6 weeks of age, when *NHERF1*$^{+/+}$ and *NHERF1*$^{-/-}$ mice showed comparable weights. The small intestine and colon were separately measured for males and females, and the length was expressed as length index, the ratio of absolute length to the body mass (Figure 1*B*). In comparison to control *NHERF1*$^{+/+}$ mice, the small intestine length index was significantly higher for *NHERF1*$^{-/-}$ male mice for all age groups and for *NHERF1*$^{-/-}$ female mice for two of three age groups (Figure 1*B*, *upper graphs*). For 12-week-old females, a trend was present, but the difference was not statistically significant. Similar results were found for the colon length index (Figure 1*B*, *middle graphs*). The body mass of *NHERF1*$^{+/+}$ and *NHERF1*$^{-/-}$ mice was equivalent at 6 weeks of age for both genders and at 12 and 24 weeks for female mice (Figure 1*B*, *lower graphs*). *NHERF1*$^{+/+}$ males showed a steeper growth curve compared to *NHERF1*$^{-/-}$ counterparts at 12 and 24 weeks of age, with statistically significant higher body masses at these time points. However, old males had equivalent body masses, whereas the weight distribution for old females, especially wild type, was scattered (Figure 1*A*).

To find out why *NHERF1*-deficient mice have longer intestines than their wild-type counterparts, we examined the expression of NHERF1 in the intestine. While it is well known that NHERF1 is expressed in IECs (Figure 2*A*, *yellow arrowhead*) [26,27], it also has high apical PM expression in the mesothelial cells of the serosa as well (Figure 2A, *arrow*) [26]. IECs result from the proliferation of intestinal stem cells through transit-amplifying/progenitor cells in the crypts followed by terminal differentiation into four mature populations: absorbtive cells, goblet cells, Paneth cells, and neuroendocrine cells [7]. The proliferation of progenitor cells was measured by BrdU incorporation and was equivalent in the crypts of *NHERF1*$^{+/+}$ and *NHERF1*$^{-/-}$ mice (Figure 2*B*). As control, splenic cells showed higher proliferation in *NHERF1*$^{-/-}$ mice. However, the localization of the *NHERF1*$^{-/-}$ BrdU-labeled progenitors appeared shifted to upper positions in the crypts. By matching the number of BrdU-positive cells with the cell position from the crypt bottom, we confirmed this observation (Figure 2*B*). This implied that there is a cell population that displaces upward the progenitor cells in the crypts. The examination of H&E small intestine sections revealed increased numbers of Paneth cells in the *NHERF1*$^{-/-}$ crypts (Figure 2*C*, *arrows*). Staining for lysozyme that specifically identifies secretory Paneth cells in crypts and with Alcian blue that highlights goblet cells showed increased numbers of both types of these secretory IECs in *NHERF1*$^{-/-}$ intestine

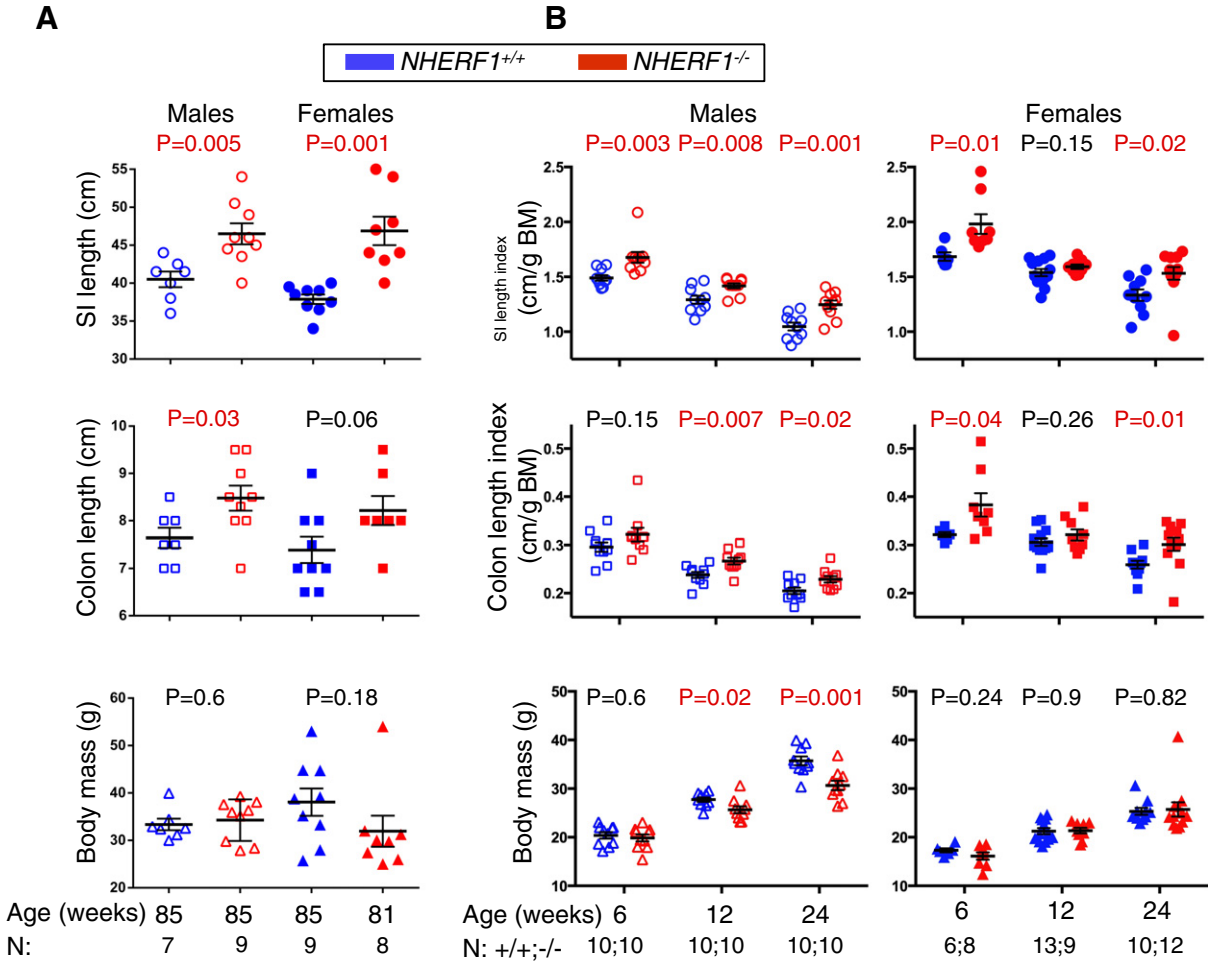

Figure 1. Increased intestinal length in *NHERF1* $^{-/-}$ mice. (A and B) The length of the small intestine (SI) and colon and the body mass (BM) were recorded at 85 weeks (A) and 6, 12, and 24 weeks of age (B) in cohorts of male and female mice. The length index was calculated as the ratio of intestine length to body mass. The SI and colon length, length index, and body mass are expressed as mean ± SEM. The groups were compared by *t* test, and the *P* values for significant differences are indicated in red. Note increased intestine length in *NHERF1* $^{-/-}$ mice as compared to control *NHERF1* $^{+/+}$ mice.

(Figure 2*C*), suggesting that NHERF1 controls the step differentiation of progenitor cells into the various populations of IECs. We have previously shown ultrastructural defects of the brush border membrane of absorbtive IECs in the ileum [19]. Ultrastructural analysis of the colon brush border revealed shorter microvilli of the *NHERF1* $^{-/-}$ colonocytes, with a length of approximately 67% the length of wild-type microvilli (Figure 2*D*), confirming previous independent findings in colon [28]. These results suggest that the alterations of IECs might be at least in part responsible for the increased intestine length of *NHERF1* $^{-/-}$ mice.

Decreased Survival and Increased Tumor Load in NHERF1 Deficient APC Mutant Mice

Pathways involved in tissue morphogenesis often play roles in tumorigenesis as well. One such pathway is the Wnt-APC-β-catenin, which is the key pathway involved in both morphogenesis and tumorigenesis in the intestine [29]. We have previously demonstrated that NHERF1 downregulation induces tumorigenic effects in human intestinal cells in 2D and 3D tissue models [14,17]. Because we found that NHERF1 is involved in intestinal morphogenesis, we explored the possibility that it may act as a tumor suppressor *in vivo* as well. *NHERF1* $^{-/-}$ mice were crossed to *Apc* $^{Min/+}$ mice, and the offspring carrying the *Min* allele were selected for survival analysis (Figure 3*A*). Double-mutant *Apc* $^{Min/+}$*NHERF1* $^{-/-}$ mice had a median survival of 19 weeks, markedly shorter than the *Apc* $^{Min/+}$*NHERF1* $^{+/+}$ counterparts. Interestingly, no significant difference was observed between the double-heterozygous *Apc* $^{Min/+}$*NHERF1* $^{+/-}$ mice and the *Apc* $^{Min/+}$*NHERF1* $^{+/+}$ mice, and their median survivals were 28 and 29 weeks, respectively. This suggests that one wild-type *NHERF1* allele is sufficient to provide adequate functional levels of NHERF1.

To study tumor development, new cohorts of *Apc* $^{Min/+}$*NHERF1* $^{+/+}$ and *Apc* $^{Min/+}$*NHERF1* $^{-/-}$ mice were sacrificed at 16 weeks (Figure 3*B*). This time point that closely precedes the median survival of double-mutant *Apc* $^{Min/+}$*NHERF1* $^{-/-}$ mice was chosen based also on a previous study showing no increase in the number of tumors detected in *Apc* $^{Min/+}$ mice after 80 days of age [30]. At 16 weeks, *Apc* $^{Min/+}$*NHERF1* $^{-/-}$ mice had lower body mass than *Apc* $^{Min/+}$*NHERF1* $^{+/+}$ mice (P = .05), most likely because of more advanced disease (Figure 3*B*). An enhanced production of IL-6 has been associated to cachexia in *Apc* $^{Min/+}$ mice [31]. All *Apc* $^{Min/+}$ mice showed signs of anemia, such as pale limbs and compensatorily enlarged spleens with increased extramedullary hematopoiesis (Figure S1). In both humans with CRC and in *Apc* $^{Min/+}$ mice, chronic bleeding due to a compromised intestinal epithelial lining leads to

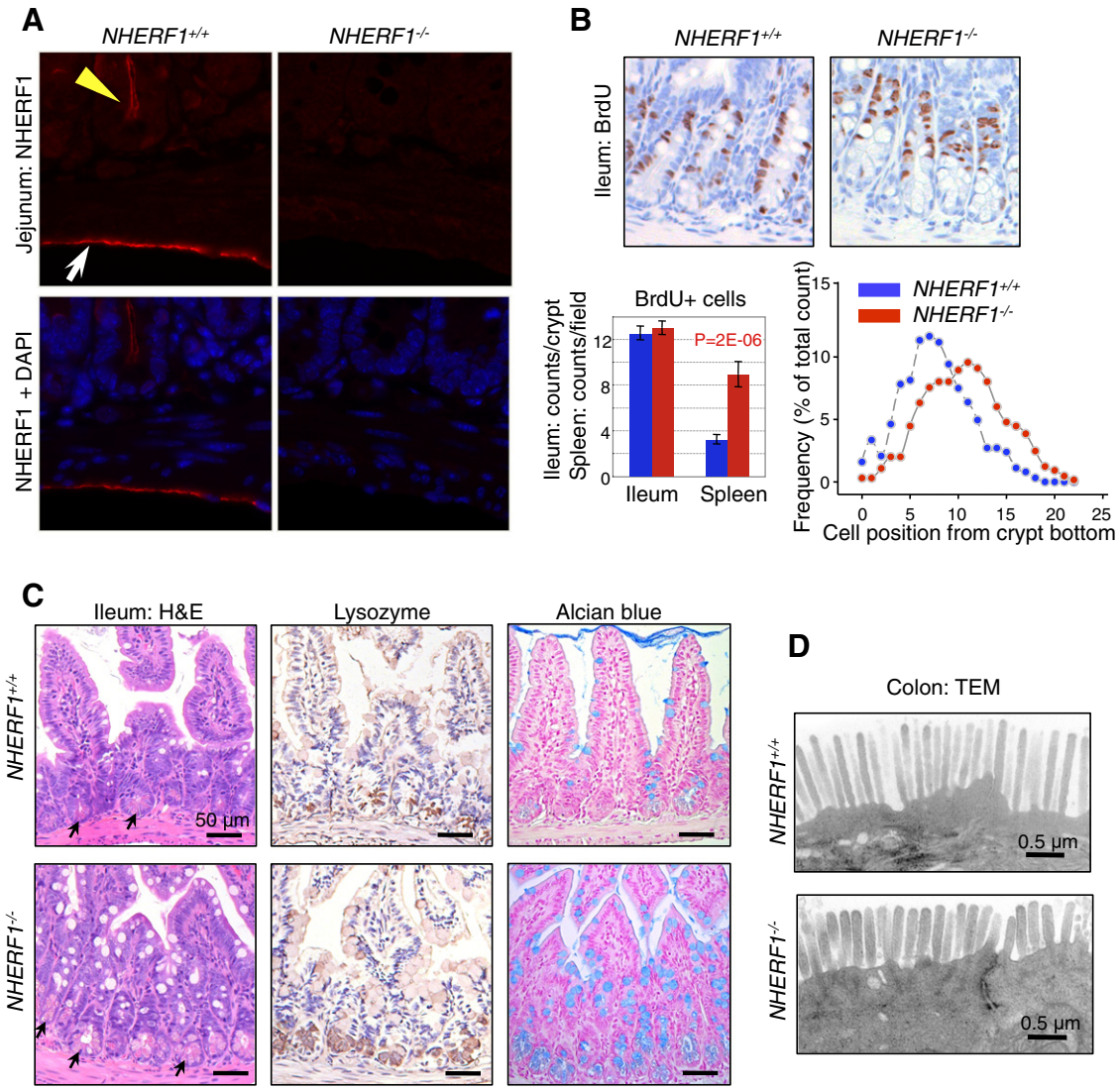

Figure 2. Intestinal defects in *NHERF1* $^{-/-}$ mice. (A) IF with NHERF1 antibody and DAPI for highlighting nuclei in *NHERF1* $^{-/-}$ and *NHERF1* $^{+/+}$ mice shows high NHERF1 apical PM expression in intestinal epithelium (yellow arrowhead) and in the mesothelial lining of the serosa (arrow). (B) BrdU incorporation in 6-week-old *NHERF1* $^{+/+}$ and *NHERF1* $^{-/-}$ female littermates showing similar numbers of BrdU+ cells in both genotypes and upper displacement of the BrdU+ progenitor cells in *NHERF1* $^{-/-}$ crypts (right graph). Data are means ± SEM from 50 crypts. The cell position 0 was assigned for the bottom-most cell of every counted crypt. In contrast, *NHERF1* $^{-/-}$ spleen BrdU+ counts show significantly enhanced proliferation. (C) H&E, lysozyme IHC for Paneth cells, and Alcian blue special stain for goblet cells of ileum sections show higher numbers of Paneth (arrows in H&E) and goblet cells in *NHERF1* $^{-/-}$ versus *NHERF1* $^{+/+}$ mice. (D) Transmission electron microscopy (TEM) shows blunted microvilli in *NHERF1* $^{-/-}$ colon epithelium.

severe anemia, which most likely precipitates death in mice [32]. The small intestine and colon were dissected and prepared as Swiss roll for histological examination (Figure S2). Neoplastic lesions, including adenomas (diameter > 1 mm) and microadenomas, were counted and the highest tumor density scored (Figures S3-S4). The double-mutant *Apc*$^{Min/+}$*NHERF1* $^{-/-}$ mice had a significantly higher tumor density in the small intestine than *Apc*$^{Min/+}$*NHERF1* $^{+/+}$ mice (Figures 3, *B* and *C* and S5). We noticed a tendency of developing more tumors in *Apc*$^{Min/+}$ females than in males, which was even more pronounced in the double-mutant mice, with statistically significant differences of 34% and 73%, respectively (Figures 3*B* and S5). The regional tumor distribution was similar for both genotypes, with an increasing gradient along its length resulting in consistently higher polyp numbers in the distal segment than in the rest of the intestine (Figure 3*D*). This distribution in C57BL/6J Apc$^{Min/+}$ mice is consistent with previous studies [33,34]. The tumorigenesis in the colon was much less developed than in the intestine, with only few or no polyps present, and a significant difference between *Apc*$^{Min/+}$*NHERF1* $^{-/-}$ and *Apc*$^{Min/+}$*NHERF1* $^{+/+}$ mice was noted only for females (Figure 3*B*).

All adenomas (diameter > 1 mm) were measured on each section level, and the highest measurement for a single tumor was scored (Figure S4). *Apc*$^{Min/+}$*NHERF1* $^{-/-}$ mice had double the number of adenomas of *Apc*$^{Min/+}$*NHERF1* $^{+/+}$ mice (Figure 3*E* and Table S2). The partition of adenomas on gender showed only slight preponderance in double-mutant females (Figure S5). Adenomas were segregated also in four consecutive size categories (Figure 3*F*). A

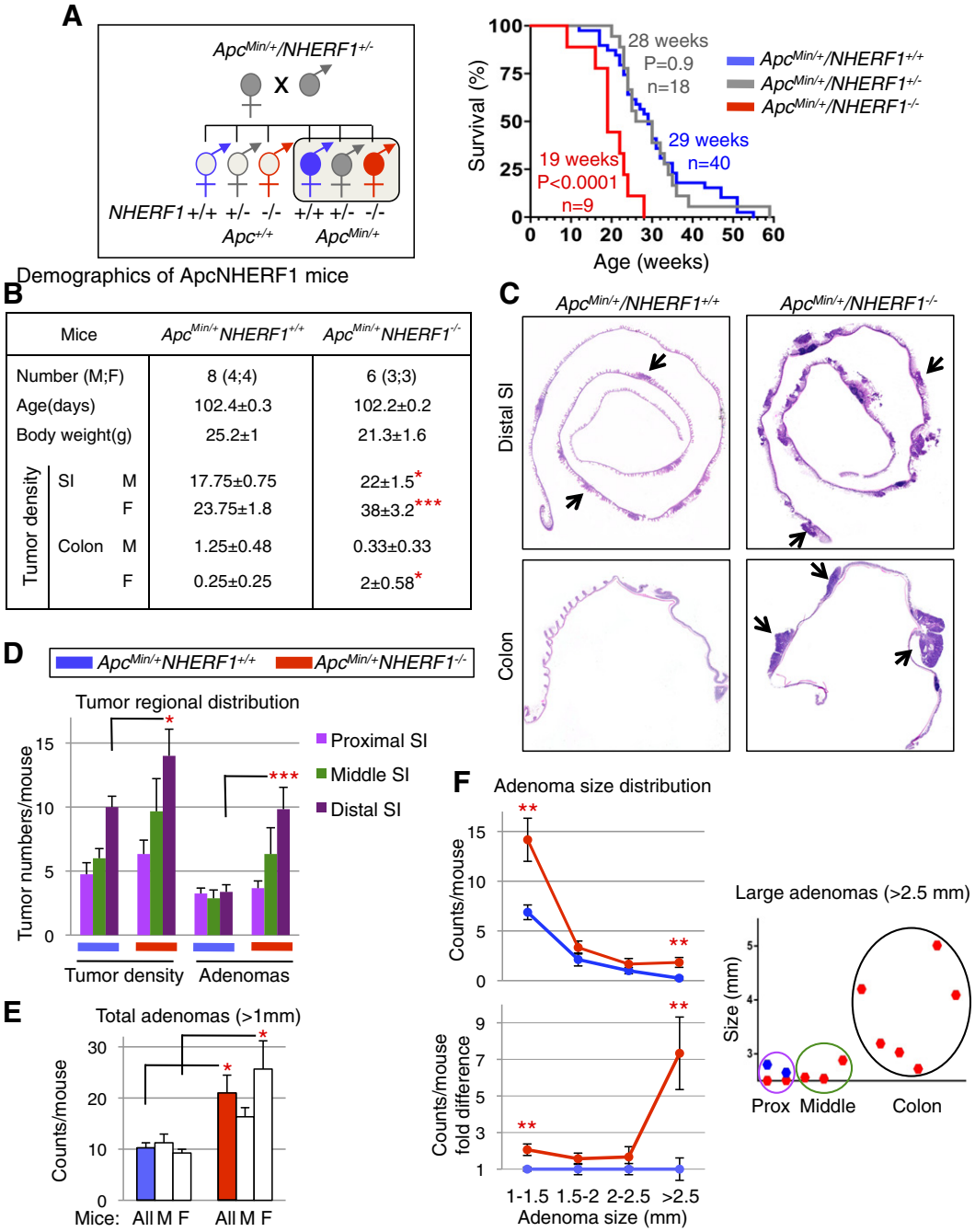

Figure 3. Decreased survival and increased intestinal tumor burden in *Apc*$^{Min/+}$*NHERF1*$^{-/-}$ double-mutant mice. (A) The diagram shows the cross between *NHERF1* and *APC* mutant mice and selection of *Apc*$^{Min/+}$ mouse cohorts (filled circles of both male and female mice) for survival and tumor burden analysis (boxed). Kaplan-Meier survival analysis shows significantly shorter survival for *Apc*$^{Min/+}$*NHERF1*$^{-/-}$ mice than for control *Apc*$^{Min/+}$*NHERF1*$^{+/+}$ mice. (B) Demographics and tumor statistical analysis in 16-week-old double-mutant and control mice shows significantly higher tumor density for *Apc*$^{Min/+}$*NHERF1*$^{-/-}$ mice in the small intestine (SI) for both males (M) and females (F), and in the colon for females. Data are means ± SEM. *$P < .05$; **$P < .01$; ***$P < .005$. (C) Swiss-roll H&E histology of distal SI and colon from two females in (B). Arrows indicate some of the polyps. Note higher tumor density and larger adenomas in *Apc*$^{Min/+}$*NHERF1*$^{-/-}$ intestine compared to control. (D–F) Tumor-count statistics performed as in (B) to demonstrate tumor regional distribution in the SI per genotype (D), adenoma numbers in the whole intestine in all mice and per gender (E), and adenoma distribution of sizes in the whole intestine (F). Adenomas were defined as tumors with diameter larger than 1 mm. The regional distribution of very large adenomas (>2.5 mm) is also shown in (F).

higher number of adenomas were noted in all the categories for the double-mutant *Apc*$^{Min/+}$*NHERF1*$^{-/-}$ mice, irrespective of gender. Strikingly, the largest tumors were on average seven times more numerous in *Apc*$^{Min/+}$*NHERF1*$^{-/-}$ mice than in *Apc*$^{Min/+}$*NHERF1*$^{+/+}$ mice (Figure 3*F*, *lower graph* and Table S2). Interestingly, the distribution of these large adenomas (>2.5 mm) was in the proximal and middle segments of the small intestine and in the colon, and attained very large sizes in double-mutant *Apc*$^{Min/+}$*NHERF1*$^{-/-}$ mice, especially in the colon (Figure 3*F*, *right graph*). In *Apc*$^{Min/+}$*NHERF1*$^{+/+}$ mice, large adenomas were seen only in the proximal segment of the

small intestine. Concurrently, the regional distribution of adenomas in these mice was blunted, indicating that most of the tumors were small at 16 weeks of age (Figure 3*D*). In contrast, the regional distribution of adenomas in $Apc^{Min/+}NHERF1^{-/-}$ mice respected the incremental gradient along the intestine, suggesting an increased tumor growth rate that parallels the rate of tumor initiation in these mice (Figure 3*D*). The histology of the tumors was that of tubular adenoma with or without high-grade dysplasia (Figure S6). Occasional gland herniation was noted at the base of the polyp but without frank invasion. Metastatic workup of liver and lung in four $Apc^{Min/+}NHERF1^{-/-}$ animals examined at the time of death did not find evidence of metastatic disease.

Overall, this analysis showed that the tumor load, including both the tumor density and tumor size, was significantly higher for both genders of the $Apc^{Min/+}NHERF1^{-/-}$ mice (Supplementary Table 2 and Figure S5), explaining the shorter survival of these animals.

Increased β-Catenin, YAP and Cyclin D1 Nuclear Localization in Tumors from NHERF1 Deficient Mice

The finding of larger adenomas in $Apc^{Min/+}NHERF1^{-/-}$ than in $Apc^{Min/+}NHERF1^{+/+}$ mice at a given time point suggested a higher growth rate for $Apc^{Min/+}NHERF1^{-/-}$ tumors. To investigate the tumor suppressor function of NHERF1 on adenoma growth, we first examined the expression levels of NHERF1 in tumors from $Apc^{Min/+}NHERF1^{+/+}$ mice. Compared to normal surrounding mucosa, both microadenomas and macroadenomas had decreased NHERF1 expression levels by IF and IHC (Figures 4*A* and S7). This result suggests a growth suppressor role of NHERF1 and is similar to results from human CRC, where NHERF1 loss from the apical PM occurs from early adenoma stage [14].

We and others have shown that NHERF1 controls tumor growth through interactions with tumor suppressor or oncogenic proteins [35] (Figure 4*B*). More specifically, NHERF1 suppresses the PI3 kinase-Akt pathway by interacting with PTEN tumor suppressor [13], and the Wnt-β-catenin pathway by interacting with β-catenin and Frizzled family members [12,16,36]. Recently, links between the Wnt-β-catenin pathway and YAP, the downstream effector of the Hippo pathway, have been revealed [11]. NHERF1 has been previously shown to interact with YAP [37], but the implications of this interaction for tumor growth have not been studied. We confirmed that NHERF1 and YAP co-immunoprecipitate and that the interaction is mediated through the PDZ2 domain of NHERF1 (Figure 4*C*), as previously reported [37]. We also found that NHERF1 interacts robustly with the YAP-S127A phosphorylation-deficient mutant (Figure 4*C*). Phosphorylation of YAP on S127 by LATS1/2, the most downstream kinases of the Hippo pathway, retains YAP in the cytoplasm, limiting its translocation to the nucleus and the transcriptional activation of genes involved in cell proliferation [11]. To investigate the role of NHERF1 in YAP signaling, we depleted NHERF1 in polarized Caco-2 CRC cells and performed subcellular fractionation (Figure 4*D*). We have previously shown that NHERF1 depletion in these cells leads to epithelial to mesenchymal transition with loss of apical cell polarity [14]. We confirmed the loss of apical polarity in NHERF1-depleted cells by the downregulation of villin, a protein involved in the structural assembly of microvilli (Figure 4*D*). In NHERF1-depleted cells, phosphorylated YAP was decreased in the cytoplasmic compartment, whereas unphosphorylated YAP was increased in the nuclear compartment (Figure 4*D*), consistent with the translocation of unphosphorylated YAP to the nucleus in the absence of NHERF1.

In human CRC cells, depletion of NHERF1 from the apical PM also results in β-catenin translocation to the nucleus, presumably due to polarity loss and epithelial to mesenchymal transition [14,17]. As previously noted in $Apc^{Min/+}$ mice, the expression of β-catenin increased in tumors compared to adjacent normal mucosa [38], and we also observed this pattern regardless of the *NHERF1* genotype. However, in $Apc^{Min/+}NHERF1^{-/-}$ mice, tumors showed higher expression of β-catenin, including nuclear β-catenin (Figure 4*E*).

In normal intestine, both phosphorylated YAP and total YAP were expressed in the crypt epithelium and not in the villi (Figure S8*A*). The aberrant crypt foci exhibited similar expression levels as the surrounding crypts (Figure S8*A*). Whereas YAP had nuclear expression in some neoplastic cells of tumors from $Apc^{Min/+}NHERF1^{-/-}$ mice (Figure 4*E*), phosphorylated YAP was mostly restricted to the cytoplasmic cell compartment of these tumors where it appeared decreased (Figure S8*B*). The findings from $Apc^{Min/+}NHERF1^{-/-}$ tumors were similar to those from Caco-2 NHERF1-depleted cells (Figure 4, *D* and *E*), suggesting that NHERF1 controls the nuclear translocation of YAP *in vivo* and *in vitro*.

Strikingly, cyclin D1, a downstream effector of the Wnt/β-catenin pathway in CRC [8] but also of the Hippo-YAP pathway [39], had prominent nuclear expression in the neoplastic glands from $Apc^{Min/+}NHERF1^{-/-}$ tumors and not in the normal mucosa (Figure 4*E*). The nuclear expression of cyclin D1 from $Apc^{Min/+}NHERF1^{-/-}$ tumors was much higher and diffuse than that seen in $Apc^{Min/+}NHERF1^{+/+}$ tumors (Figure 4*E*), explaining the faster growth rate of the $Apc^{Min/+}NHERF1^{-/-}$ tumors. Although NHERF1 is a positive regulator of PTEN tumor suppressor [13] and PTEN suppresses cyclin D1 levels [40], we could not find elevated phosphorylated Akt by IHC in the tumors examined (not shown).

Analysis of YAP and Phosphorylated YAP Expression in Matched Normal-Adenoma-Carcinoma Specimens of Human CRC

We have previously shown in matched normal-adenoma-carcinoma specimens that NHERF1 membrane expression is lost early in adenoma and that loss or cytoplasmic overexpression is present in carcinoma [14]. Examination of the expression levels of phosphorylated YAP in the same series of frozen specimens by Western blot showed a sharp drop from early initial adenoma stages (Figure 5*A*). Total YAP expression levels decreased much less and more gradually in the sequence normal-adenoma-carcinoma, resulting in a relative decrease of phosphorylated YAP as compared to total YAP (Figure 5*A*, *upper graph*). IHC of resection specimens with normal, adenoma, and carcinoma histology on the same slide showed a marked increase of YAP nuclear staining from normal to adenoma and carcinoma stages, with moderate and prominent nuclear staining in adenoma and carcinoma, respectively (Figure 5*B*, *lower panels*). This suggested activation of the transcriptional growth program regulated by YAP. IHC with P-YAP antibody showed the presence of phosphorylated YAP in the cytoplasm of cells in normal, adenoma, and carcinoma tissues with similar levels in adenoma and carcinoma (Figure 5*B*, *middle panels*). Occasional moderate nuclear staining was noted in adenoma and carcinoma. In some cases, the levels of phosphorylated YAP appeared lower in normal epithelial cells, as in the case depicted in Figure 5*B*. Interestingly, the smooth muscle of muscularis mucosae and of the small arteries in the submucosa expressed phosphorylated YAP in the cytoplasm (Figure 5*B*, *arrows*). As these components are usually present in a normal mucosal biopsy, the high levels of phosphorylated YAP noted in the normal

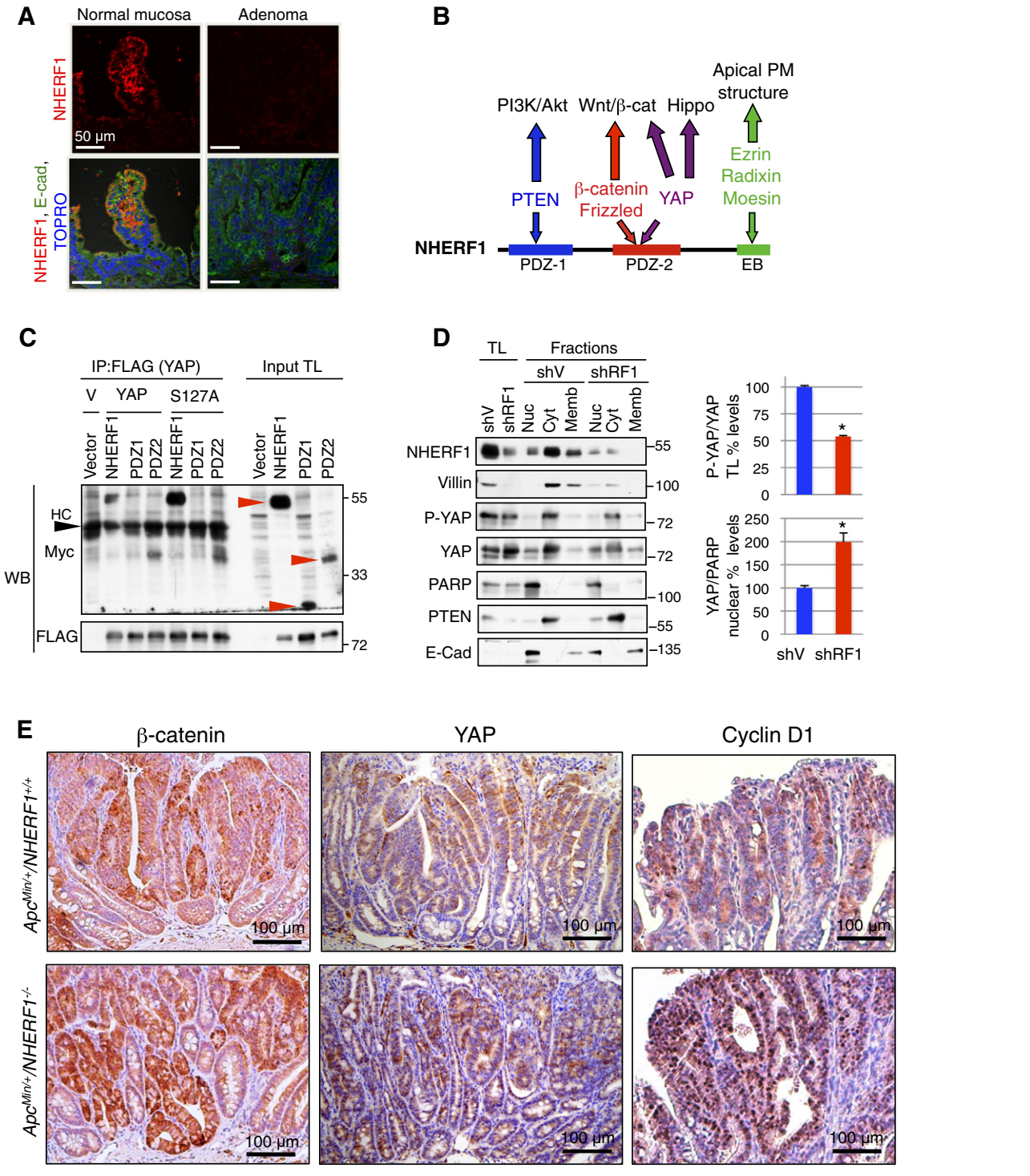

Figure 4. *NHERF1* deficiency promotes nuclear localization of β-catenin, YAP, and cyclin D1. (A) IF analysis of $Apc^{Min/+}NHERF1^{+/+}$ normal mucosa and adenomas with antibodies indicated on the left and TOPRO-3 highlighting nuclei shows strong NHERF1 expression at the apical PM of enterocytes from normal mucosa and loss of expression in adenoma. (B) Schematic domain structure of NHERF1 showing interactions with selected ligands involved in tumor growth and the pathways they control. EB, ERM-binding region. (C) Co-immunoprecipitation (IP) of proteins (400 μg) from total lysates (TL) of 293T cells coexpressing FLAG-tagged YAP wild type or YAP-S127A phosphorylation-deficient mutant and Myc-tagged NHERF1 full length and separate PDZ domains (red arrowheads). HC, heavy chain. V, YAP plasmid vector. Note interaction between NHERF1 full length or PDZ2 with either YAP wild type or S127A mutant. (D) Subcellular fractionation in nuclear (Nuc), cytoplasmic (Cyt), and membrane (Memb) fractions of Caco-2 CRC cells infected with either shRNA vector (shV) or shRNA-1 NHERF1 (shRF1). Proteins from total cell lysates (TL) and subcellular fractions were loaded at 20 μg per lane. PARP, PTEN, and E-cadherin were used as nuclear, cytoplasmic, and membrane fractionation markers, respectively. By using this procedure, it is known that cross contamination may occur between the nuclear fraction and membrane components, whereas the cytoplasmic fraction is pure. Normalized phosphorylated YAP (P-YAP) to YAP expression in total lysates and normalized nuclear YAP to PARP expression are represented as mean ± SD in control and NHERF1 knockdown Caco-2 cells. *$P < .05$. E. IHC with β-catenin, YAP, and cyclin D1 antibodies shows higher expression of these proteins in $Apc^{Min/+}NHERF1^{-/-}$ tumors compared to control. Nuclear expression is elevated for β-catenin and YAP in $Apc^{Min/+}NHERF1^{-/-}$ tumors, and very prominent for cyclin D1.

tissue from the frozen specimens (Figure 5*A*) may in part be due to the smooth muscle cells. However, normalization of these levels to total YAP, also present in the same smooth muscle cell compartments (Figure 5*B*, *arrows*), most likely reflected the fraction of YAP that is phosphorylated overall. Altogether, the relative decrease of phosphorylated YAP and the increase of YAP nuclear expression in human CRC samples were in concordance with the observations from *Apc*$^{Min/+}$*NHERF1*$^{-/-}$ mice.

Discussion

In this study, we examined the effect of NHERF1 deficiency on intestinal tumorigenesis in order to explore the significance of the loss of NHERF1 that we have reported in human CRC [14]. NHERF1 deficiency as a single hit in mice does not lead to intestinal polyposis. Old mice have increased lymphoid proliferation in many organs, including in the gut-associated lymphoid tissue, and NHERF1 deficiency increases the intensity of this process. NHERF1-deficient

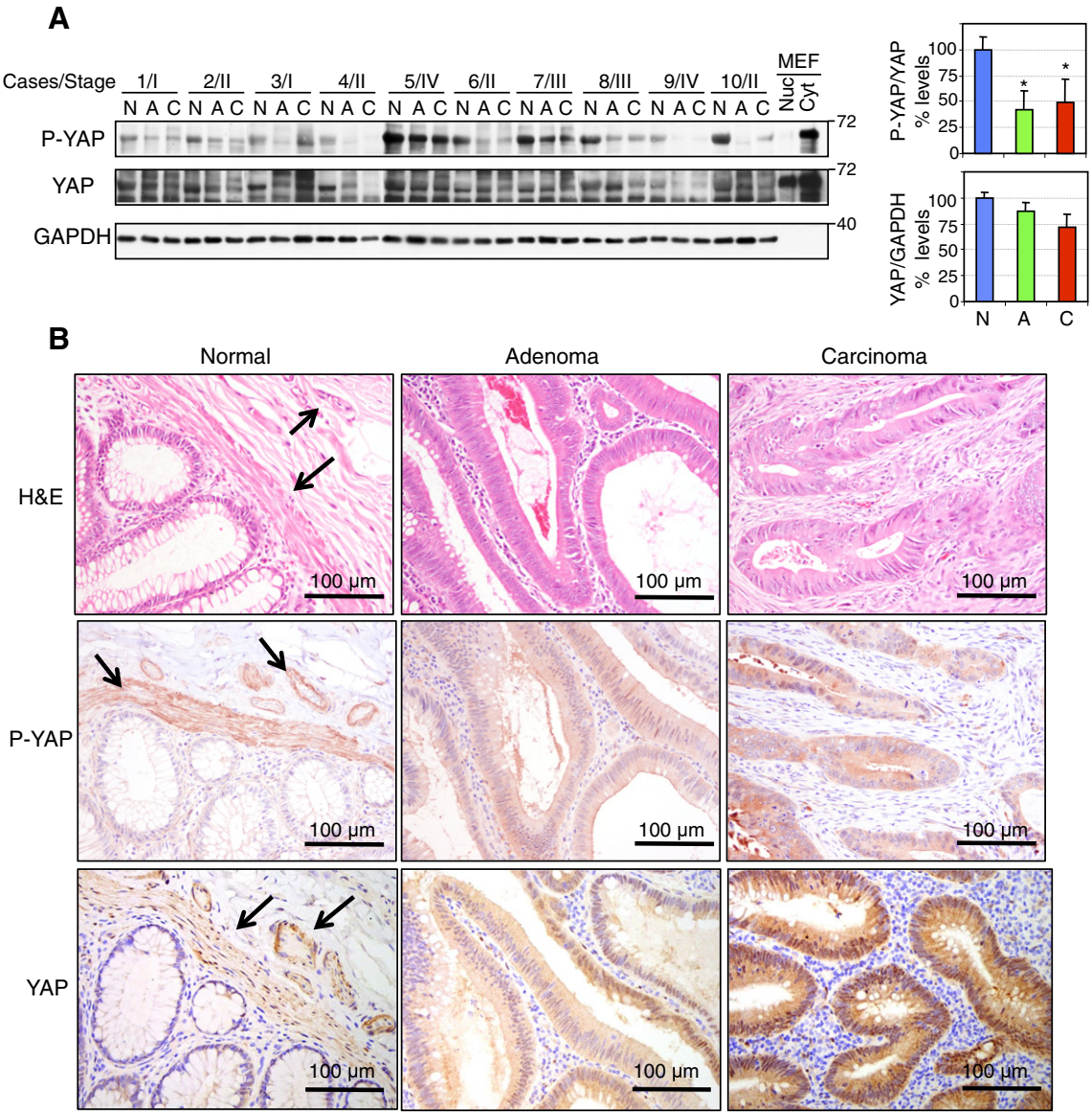

Figure 5. Progressive changes of YAP phosphorylation and expression in CRC. (A) Western blot with phosphorylated YAP (S127) (P-YAP) and total YAP antibodies of proteins (20 μg) from whole tissue lysates from frozen matched sets of normal (N), adenoma (A), and carcinoma (C) samples shows decrease of phosphorylated YAP from adenoma stages in the progression of CRC. AJCC stage is indicated for each case. The filters were first probed with P-YAP antibody, stripped, and probed with YAP antibody. Both antibodies recognized a band corresponding to the YAP65 isoform that contains only one WW domain and is expressed in nuclear (Nuc) and cytoplasmic (Cyt) extracts of mouse embryonic fibroblasts (MEFs). A separate run was performed for control GAPDH. Normalized phosphorylated YAP (P-YAP) to YAP expression and normalized YAP to GAPDH expression are represented as mean ± SD. *$P < .01$ versus normal tissue. (B) IHC analysis with P-YAP and YAP antibodies of resection specimens containing adjacent areas of normal mucosa, adenoma, and carcinoma on the same slide shows expression of both forms in the normal epithelial cells but also in the smooth muscle cells of the muscularis mucosae and arteries media (arrows). P-YAP is mostly confined to the cytoplasmic compartment, and YAP stains the cytoplasm and some nuclei. Note increased YAP staining of both subcellular compartments in carcinoma.

mice have nevertheless morphological defects of both small intestine and colon, including attenuated brush border of absorptive IECs, increased numbers of secretory IECs, and significantly increased length. The latter reaches 24% increase for aged females (at 84% of wild-type body mass) and 15% increase for aged males (at 103% of wild-type body mass) in the small intestine, and 11% increase for both genders in the colon. Smaller but significant differences are also detected in very young mice, arguing for a combination of developmental and adaptive determining factors. NHERF1 interacts with and regulates the activity of ion exchangers and channels, such as NHE3 and CFTR [28,41–43] that are expressed in the intestinal brush border. *NHE3*-deficient mice have absorptive defects and compensatory enlarged small intestine and colon, although by distension rather than by increased segmental length [44]. *CFTR* mutant mice have increased numbers of goblet cells in the ileum similar to *NHERF1*-deficient mice, and mildly increased small intestine length (by 10%) [45,46]. To our knowledge, the increase in intestinal length in the *NHERF1*-deficient mice is the highest reported, being most likely due to contributions from an altered mucosa and possibly serosa.

As this is the first demonstration of the tumor suppressor role of NHERF1 *in vivo*, we undertook a thorough analysis of the tumorigenesis in the intestine. NHERF1 deficiency in the context of the *APC* mutation in $Apc^{Min/+}$ mice leads to drastic shortening of the survival of double-mutant mice due to significantly increased tumor load. The complete absence of NHERF1 expression is required for tumorigenesis, as heterozygous *NHERF1* mice do not show a different phenotype from *NHERF1* wild-type mice. One intriguing observation in our cohorts was the difference in tumorigenesis between $Apc^{Min/+}$ male and female mice. The tumor density was increased in female mice of both genotypes, whereas adenomas developed at a similar rate in both genders in $Apc^{Min/+}$ mice and yet again with female predominance in $Apc^{Min/+}NHERF1^{-/-}$ double-mutant mice. One correlation is the regulation of NHERF1 expression by estrogen receptor [47] and its variation in rodent intestine during estral cycle [48]. Although this could explain the limited growth of adenomas in $Apc^{Min/+}$ females by a suppressor effect of NHERF1, more studies are necessary to address the increased tumor incidence in $Apc^{Min/+}$ females. Interestingly, NHERF2, the homolog of NHERF1, appears to have an opposite role in tumorigenesis, as double-mutant $Apc^{Min/+}NHERF2^{-/-}$ mice develop smaller albeit not fewer tumors than $Apc^{Min/+}$ controls [49].

Comparison to other mutant mice on $Apc^{Min/+}$ background showed that the tumorigenesis in *NHERF1*-deficient mice best resembles the one developing in the cyclin-dependent-kinase (cdk) inhibitor *Cdkn1b* (p27)-deficient mice [34,50], except that the latter shows gene dosage dependence. Similarly to p27, NHERF1 deficiency results in a moderately increased tumor incidence but a marked increase in the number of large adenomas. Also like p27, NHERF1 expression is reduced in tumors from single-mutant $Apc^{Min/+}$ mice, suggesting causal relationship to tumor growth. Although cyclin D1 expression has not been investigated in *Cdkn1b*-deficient mice, the mitotic index was increased in tumors from these mice, consistent with increased tumor cell proliferation [34]. In *NHERF1*-deficient mice, the expression and nuclear localization of cyclin D1 were massively increased in tumors, suggesting accelerated cell cycle progression and growth. Indeed, the role of cyclin D1 for tumor growth but not tumor initiation following *APC* loss in the intestine has been established, as *cyclin D1*–deficient mice develop the same number of tumors as matched controls but fail to develop adenomas, defined as lesions with diameter > 1 mm, as in our study [51].

Analysis of possible pathways upstream of cyclin D1 upregulation in $Apc^{Min/+}NHERF1^{-/-}$ tumors showed elevated levels of cytoplasmic and nuclear β-catenin and elevated levels of nuclear YAP. The involvement of these pathways downstream of NHERF1 may explain not only the intestinal oncogenesis from *NHERF1*-deficient mice but perhaps some of the morphological defects, such as increased numbers of secretory cells. YAP has been recently shown to promote the differentiation of intestinal stem cells into goblet cells [52], and Wnt overactivation by APC loss leads to overproduction of Paneth cells [53]. Interestingly, *CFTR* mutant mice that share some similar morphological intestinal defects as *NHERF1*-deficient mice have also increased intestinal tumorigenesis on an $Apc^{Min/+}$ background that may be due to increased Wnt -β-catenin pathway [54].

Mechanistically, NHERF1 interacts through its PDZ2 domain with both β-catenin and YAP [12,37], and a direct interaction between NHERF1 and some members of the Frizzled family has also been documented [36] (Figure 4*B*). We have previously shown that NHERF1 contributes to the stabilization of E-cadherin–β-catenin complexes at the PM in mouse embryonic fibroblasts and also human CRC cells [14,16]. *NHERF1* deficiency leads to E-cadherin and β-catenin drop from the PM, increase in cytoplasmic and nuclear β-catenin, and β-catenin promoter transactivation [16]. The interaction between NHERF1 and YAP has been involved in the compartmentalization of YAP at the apical PM in polarized airway epithelial cells [37]. We have shown here that NHERF1 deficiency, either by shRNA knockdown in CRC cells or by gene knockout in mice, leads to accumulation of unphosphorylated active YAP that most likely contributes to tumorigenesis either by inducing target genes of the transcriptional YAP/TAZ-TEAD complex or by entering in a transcriptional complex containing β-catenin [11] (Figure 4*B*). The nuclear expression of unphosphorylated YAP was also confirmed in human CRC samples. Although YAP has been found at the apical PM in airway cells [37], it is mainly distributed in the cytoplasm of normal crypt cells in the intestine. Whether the mechanism of YAP nuclear translocation involves direct interaction between the cytoplasmic fractions of NHERF1 and YAP with sequestration of the unphosphorylated YAP fraction in the cytoplasm or a more indirect signaling involving YAP dephosphorylation [55] is unknown at the present time.

In conclusion, we show here that NHERF1 loss from the PM is oncogenic *in vivo* through its influence on Wnt-APC-β-catenin and Hippo-YAP pathways. Further *in vivo* studies are required to extend this role to other malignancies dependent of the Wnt-β-catenin pathway and to dissect the functions of NHERF1 in other subcellular locations. The understanding of the function of NHERF1 will trigger the refinement of the ongoing therapeutic efforts for modulating its activity [56,57].

Acknowledgements

The authors thank Erica Kreimann and Clifton Stephens for help with the analysis of aged mice and Kenneth Dunner for help with electron microscopy.

This work was supported by the National Cancer Institute CA107201 grant and MD Anderson Cancer Center G. S. Hogan Gastrointestinal Research Fund to M. M. G. Animal breeding and tissue processing were partly supported by the National Cancer Institute CA16672 grant and by the National Institutes of Health Public Health Service grant P30-DK56338 (funding the Texas Medical Center Digestive Disease Center), respectively.

Appendix A. Supplementary Data

Supplementary data to this article can be found online at http://dx.doi.org/10.1016/j.neo.2016.07.003.

References

[1] Jemal A, Murray T, Ward E, Samuels A, Tiwari RC, Ghafoor A, Feuer EJ, and Thun MJ (2005). Cancer statistics, 2005. *CA Cancer J Clin* **55**, 10–30.

[2] Brenner H, Kloor M, and Pox CP (2014). Colorectal cancer. *Lancet* **383**, 1490–1502.

[3] Vogelstein B and Kinzler KW (2004). Cancer genes and the pathways they control. *Nat Med* **10**, 789–799.

[4] Gregorieff A, Pinto D, Begthel H, Destree O, Kielman M, and Clevers H (2005). Expression pattern of Wnt signaling components in the adult intestine. *Gastroenterology* **129**, 626–638.

[5] He X, Semenov M, Tamai K, and Zeng X (2004). LDL receptor–related proteins 5 and 6 in Wnt/beta-catenin signaling: arrows point the way. *Development* **131**, 1663–1677.

[6] Tolwinski NS, Wehrli M, Rives A, Erdeniz N, DiNardo S, and Wieschaus E (2003). Wg/Wnt signal can be transmitted through arrow/LRP5,6 and Axin independently of Zw3/Gsk3beta activity. *Dev Cell* **4**, 407–418.

[7] Crosnier C, Stamataki D, and Lewis J (2006). Organizing cell renewal in the intestine: stem cells, signals and combinatorial control. *Nat Rev Genet* **7**, 349–359.

[8] Tetsu O and McCormick F (1999). Beta-catenin regulates expression of cyclin D1 in colon carcinoma cells. *Nature* **398**, 422–426.

[9] Parsons DW, Wang TL, Samuels Y, Bardelli A, Cummins JM, DeLong L, Silliman N, Ptak J, Szabo S, and Willson JK, et al (2005). Colorectal cancer: mutations in a signalling pathway. *Nature* **436**, 792.

[10] Azzolin L, Panciera T, Soligo S, Enzo E, Bicciato S, Dupont S, Bresolin S, Frasson C, Basso G, and Guzzardo V, et al (2014). YAP/TAZ incorporation in the beta-catenin destruction complex orchestrates the Wnt response. *Cell* **158**, 157–170.

[11] Hansen CG, Moroishi T, and Guan KL (2015). YAP and TAZ: a nexus for Hippo signaling and beyond. *Trends Cell Biol* **25**, 499–513.

[12] Shibata T, Chuma M, Kokubu A, Sakamoto M, and Hirohashi S (2003). EBP50, a beta-catenin-associating protein, enhances Wnt signaling and is over-expressed in hepatocellular carcinoma. *Hepatology* **38**, 178–186.

[13] Takahashi Y, Morales FC, Kreimann EL, and Georgescu MM (2006). PTEN tumor suppressor associates with NHERF proteins to attenuate PDGF receptor signaling. *EMBO J* **25**, 910–920.

[14] Hayashi Y, Molina JR, Hamilton SR, and Georgescu MM (2010). NHERF1/EBP50 is a new marker in colorectal cancer. *Neoplasia* **12**, 1013–1022.

[15] Malfettone A, Silvestris N, Paradiso A, Mattioli E, Simone G, and Mangia A (2012). Overexpression of nuclear NHERF1 in advanced colorectal cancer: association with hypoxic microenvironment and tumor invasive phenotype. *Exp Mol Pathol* **92**, 296–303.

[16] Kreimann EL, Morales FC, de Orbeta-Cruz J, Takahashi Y, Adams H, Liu TJ, McCrea PD, and Georgescu MM (2007). Cortical stabilization of beta-catenin contributes to NHERF1/EBP50 tumor suppressor function. *Oncogene* **26**, 5290–5299.

[17] Georgescu MM, Cote G, Agarwal NK, and White III CL (2014). NHERF1/EBP50 controls morphogenesis of 3D colonic glands by stabilizing PTEN and ezrin-radixin-moesin proteins at the apical membrane. *Neoplasia* **16**, 365–374.

[18] McCart AE, Vickaryous NK, and Silver A (2008). Apc mice: models, modifiers and mutants. *Pathol Res Pract* **204**, 479–490.

[19] Morales FC, Takahashi Y, Kreimann EL, and Georgescu MM (2004). Ezrin-radixin-moesin (ERM)-binding phosphoprotein 50 organizes ERM proteins at the apical membrane of polarized epithelia. *Proc Natl Acad Sci U S A* **101**, 17705–17710.

[20] Morales FC, Hayashi Y, van Pelt CS, and Georgescu MM (2012). NHERF1/EBP50 controls lactation by establishing basal membrane polarity complexes with prolactin receptor. *Cell Death Dis* **3**e391.

[21] Boivin GP, Washington K, Yang K, Ward JM, Pretlow TP, Russell R, Besselsen DG, Godfrey VL, Doetschman T, and Dove WF, et al (2003). Pathology of mouse models of intestinal cancer: consensus report and recommendations. *Gastroenterology* **124**, 762–777.

[22] Molina JR, Agarwal NK, Morales FC, Hayashi Y, Aldape KD, Cote G, and Georgescu MM (2012). PTEN, NHERF1 and PHLPP form a tumor suppressor network that is disabled in glioblastoma. *Oncogene* **31**, 1264–1274.

[23] Georgescu MM, Kirsch KH, Akagi T, Shishido T, and Hanafusa H (1999). The tumor-suppressor activity of PTEN is regulated by its carboxyl-terminal region. *Proc Natl Acad Sci U S A* **96**, 10182–10187.

[24] Georgescu MM, Yell P, Mobley BC, Shang P, Georgescu T, Wang SH, Canoll P, Hatanpaa KJ, White 3rd CL, and Raisanen JM (2015). NHERF1/EBP50 is an organizer of polarity structures and a diagnostic marker in ependymoma. *Acta Neuropathol Commun* **3**, 11.

[25] Kamiya K, Michel V, Giraudet F, Riederer B, Foucher I, Papal S, Perfettini I, Le Gal S, Verpy E, and Xia W, et al (2014). An unusually powerful mode of low-frequency sound interference due to defective hair bundles of the auditory outer hair cells. *Proc Natl Acad Sci U S A* **111**, 9307–9312.

[26] Ingraffea J, Reczek D, and Bretscher A (2002). Distinct cell type–specific expression of scaffolding proteins EBP50 and E3KARP: EBP50 is generally expressed with ezrin in specific epithelia, whereas E3KARP is not. *Eur J Cell Biol* **81**, 61–68.

[27] Stemmer-Rachamimov AO, Wiederhold T, Nielsen GP, James M, Pinney-Michalowski D, Roy JE, Cohen WA, Ramesh V, and Louis DN (2001). NHE-RF, a merlin-interacting protein, is primarily expressed in luminal epithelia, proliferative endometrium, and estrogen receptor-positive breast carcinomas. *Am J Pathol* **158**, 57–62.

[28] Broere N, Chen M, Cinar A, Singh AK, Hillesheim J, Riederer B, Lunnemann M, Rottinghaus I, Krabbenhoft A, and Engelhardt R, et al (2009). Defective jejunal and colonic salt absorption and alteredNa(+)/H (+) exchanger 3 (NHE3) activity in NHE regulatory factor 1 (NHERF1) adaptor protein-deficient mice. *Pflugers Arch - Eur J Physiol* **457**, 1079–1091.

[29] de Lau W, Barker N, and Clevers H (2007). WNT signaling in the normal intestine and colorectal cancer. *Front Biosci* **12**, 471–491.

[30] Fazeli A, Steen RG, Dickinson SL, Bautista D, Dietrich WF, Bronson RT, Bresalier RS, Lander ES, Costa J, and Weinberg RA (1997). Effects of p53 mutations on apoptosis in mouse intestinal and human colonic adenomas. *Proc Natl Acad Sci U S A* **94**, 10199–10204.

[31] Baltgalvis KA, Berger FG, Pena MM, Davis JM, Muga SJ, and Carson JA (2008). Interleukin-6 and cachexia in ApcMin/+ mice. *Am J Phys Regul Integr Comp Phys* **294**, R393-401.

[32] Su LK, Kinzler KW, Vogelstein B, Preisinger AC, Moser AR, Luongo C, Gould KA, and Dove WF (1992). Multiple intestinal neoplasia caused by a mutation in the murine homolog of the APC gene. *Science* **256**, 668–670.

[33] Haigis KM, Hoff PD, White A, Shoemaker AR, Halberg RB, and Dove WF (2004). Tumor regionality in the mouse intestine reflects the mechanism of loss of Apc function. *Proc Natl Acad Sci U S A* **101**, 9769–9773.

[34] Philipp-Staheli J, Kim KH, Payne SR, Gurley KE, Liggitt D, Longton G, and Kemp CJ (2002). Pathway-specific tumor suppression. Reduction of p27 accelerates gastrointestinal tumorigenesis in Apc mutant mice, but not in Smad3 mutant mice. *Cancer Cell* **1**, 355–368.

[35] Georgescu MM, Morales FC, Molina JR, and Hayashi Y (2008). Roles of NHERF1/EBP50 in cancer. *Curr Mol Med* **8**, 459–468.

[36] Wheeler DS, Barrick SR, Grubisha MJ, Brufsky AM, Friedman PA, and Romero G (2011). Direct interaction between NHERF1 and Frizzled regulates beta-catenin signaling. *Oncogene* **30**, 32–42.

[37] Mohler PJ, Kreda SM, Boucher RC, Sudol M, Stutts MJ, and Milgram SL (1999). Yes-associated protein 65 localizes p62(c-Yes) to the apical compartment of airway epithelia by association with EBP50. *J Cell Biol* **147**, 879–890.

[38] Pinto D and Clevers H (2005). Wnt control of stem cells and differentiation in the intestinal epithelium. *Exp Cell Res* **306**, 357–363.

[39] Imajo M, Miyatake K, Iimura A, Miyamoto A, and Nishida E (2012). A molecular mechanism that links Hippo signalling to the inhibition of Wnt/beta-catenin signalling. *EMBO J* **31**, 1109–1122.

[40] Radu A, Neubauer V, Akagi T, Hanafusa H, and Georgescu MM (2003). PTEN induces cell cycle arrest by decreasing the level and nuclear localization of cyclin D1. *Mol Cell Biol* **23**, 6139–6149.

[41] Broere N, Hillesheim J, Tuo B, Jorna H, Houtsmuller AB, Shenolikar S, Weinman EJ, Donowitz M, Seidler U, and de Jonge HR, et al (2007). Cystic fibrosis transmembrane conductance regulator activation is reduced in the small intestine of Na+/H+ exchanger 3 regulatory factor 1 (NHERF-1)– but not NHERF-2–deficient mice. *J Biol Chem* **282**, 37575–37584.

[42] Wang S, Raab RW, Schatz PJ, Guggino WB, and Li M (1998). Peptide binding consensus of the NHE-RF-PDZ1 domain matches the C-terminal sequence of cystic fibrosis transmembrane conductance regulator (CFTR). *FEBS Lett* **427**, 103–108.

[43] Weinman EJ, Steplock D, Wang Y, and Shenolikar S (1995). Characterization of a protein cofactor that mediates protein kinase A regulation of the renal brush border membrane Na(+)-H+ exchanger. *J Clin Invest* **95**, 2143–2149.

[44] Schultheis PJ, Clarke LL, Meneton P, Miller ML, Soleimani M, Gawenis LR, Riddle TM, Duffy JJ, Doetschman T, and Wang T, et al (1998). Renal and intestinal absorptive defects in mice lacking the NHE3 Na+/H+ exchanger. *Nat Genet* **19**, 282–285.

[45] Ohlsson L, Hjelte L, Huhn M, Scholte BJ, Wilke M, Flodstrom-Tullberg M, and Nilsson A (2008). Expression of intestinal and lung alkaline sphingomyelinase and neutral ceramidase in cystic fibrosis f508del transgenic mice. *J Pediatr Gastroenterol Nutr* **47**, 547–554.

[46] Wilke M, Buijs-Offerman RM, Aarbiou J, Colledge WH, Sheppard DN, Touqui L, Bot A, Jorna H, de Jonge HR, and Scholte BJ (2011). Mouse models of cystic fibrosis: phenotypic analysis and research applications. *J Cyst Fibros* **10**(Suppl. 2), S152–S171.

[47] Ediger TR, Kraus WL, Weinman EJ, and Katzenellenbogen BS (1999). Estrogen receptor regulation of the Na+/H+ exchange regulatory factor. *Endocrinology* **140**, 2976–2982.

[48] Cuello-Carrion FD, Troncoso M, Guinazu E, Valdez SR, Fanelli MA, Ciocca DR, and Kreimann EL (2010). Estrogens regulate the expression of NHERF1 in normal colon during the reproductive cycle of Wistar rats. *Histochem Cell Biol* **134**, 623–630.

[49] Yoshida M, Zhao L, Grigoryan G, Shim H, He P, and Yun CC (2016). Deletion of Na+/H+ exchanger regulatory factor 2 represses colon cancer progress by suppression of Stat3 and CD24. *Am J Physiol Gastrointest Liver Physiol* **310**, G586–G598.

[50] Taketo MM and Edelmann W (2009). Mouse models of colon cancer. *Gastroenterology* **136**, 780–798.

[51] Sansom OJ, Reed KR, van de Wetering M, Muncan V, Winton DJ, Clevers H, and Clarke AR (2005). Cyclin D1 is not an immediate target of beta-catenin following Apc loss in the intestine. *J Biol Chem* **280**, 28463–28467.

[52] Imajo M, Ebisuya M, and Nishida E (2015). Dual role of YAP and TAZ in renewal of the intestinal epithelium. *Nat Cell Biol* **17**, 7–19.

[53] Sansom OJ, Reed KR, Hayes AJ, Ireland H, Brinkmann H, Newton IP, Batlle E, Simon-Assmann P, Clevers H, and Nathke IS, et al (2004). Loss of Apc in vivo immediately perturbs Wnt signaling, differentiation, and migration. *Genes Dev* **18**, 1385–1390.

[54] Than BL, Linnekamp JF, Starr TK, Largaespada DA, Rod A, Zhang Y, Bruner V, Abrahante J, Schumann A, and Luczak T, et al (2016). CFTR is a tumor suppressor gene in murine and human intestinal cancer. *Oncogene*.

[55] Kremer KN, Dudakovic A, Hess AD, Smith BD, Karp JE, Kaufmann SH, Westendorf JJ, van Wijnen AJ, and Hedin KE (2015). Histone deacetylase inhibitors target the leukemic microenvironment by enhancing a Nherf1-protein phosphatase 1alpha-TAZ signaling pathway in osteoblasts. *J Biol Chem* **290**, 29478–29492.

[56] Fitzpatrick JM, Pellegrini M, Cushing PR, and Mierke DF (2014). Small molecule inhibition of the Na(+)/H(+) exchange regulatory factor 1 and parathyroid hormone 1 receptor interaction. *Biochemistry* **53**, 5916–5922.

[57] Mayasundari A, Ferreira AM, He L, Mahindroo N, Bashford D, and Fujii N (2008). Rational design of the first small-molecule antagonists of NHERF1/EBP50 PDZ domains. *Bioorg Med Chem Lett* **18**, 942–945.